2026 IEEE/SICE International Symposium on System Integration (SII)
January 11-14, 2026. Cancún, México

FEM-Based Optimization of the Mechanical Properties of a Soft Robotic Neck

Alberto Rodríguez–Sanz[1*], Gerson Lipa[1*], Baptiste Rouquette[2], Jorge Muñoz[1] and Concepción A. Monje[1]

***Abstract*— Finite element modeling (FEM) provides a powerful and flexible approach for accurately simulating soft robots and their dynamics. This work presents a simulation-based framework for identifying the mechanical properties of a 3D-printed, cable-driven soft robotic neck made of thermoplastic polyurethane (TPU) with a Shore hardness of 82A. A Bayesian optimization method is employed during FEM simulations in the open-source SOFA framework to estimate material parameters by minimizing the discrepancy between experimental data and simulation results. Cyclic traction tests were conducted on a custom test bench to obtain force and displacement data from one of the three actuation cables of the neck. Based on these observations, a hyperelastic constitutive model was selected, and its parameters optimized. The simulated response remained consistent with experimental measurements, indicating that the model captures the essential mechanical behavior of the system. This approach opens a practical alternative to direct material characterization and lays the foundation for future extensions involving viscoplastic models adaptive force–based control.**

I. INTRODUCTION

Soft robots are a class of compliant systems inspired by biological structures and built from elastomeric materials such as silicone or thermoplastic polyurethanes (TPU). Their inherent flexibility enables safe interaction with humans, adaptability to complex environments, and execution of tasks that require continuous deformation. As these systems become more sophisticated, accurately modeling their mechanical behavior is essential for design, control and simulation.

To address this challenge, several modeling approaches have been proposed. Geometric formulations such as the Piecewise Constant Curvature (PCC) model [1], [2] offer computational efficiency and are widely used in real–time control, but their accuracy degrades under external loads or nonuniform deformations. Data-driven strategies, including neural networks and physics–informed neural networks (PINNs) [3], provide accurate mappings from data but require extensive training and exhibit limited generalization outside trained scenarios.

An alternative to both of these approaches is the Finite Element Method (FEM), which computes the deformation of soft structures based on continuum mechanics. By explicitly encoding geometry and material properties, FEM captures complex strain distributions and contact interactions without relying on restrictive assumptions [4]. However, FEM also presents limitations: its computational cost grows with mesh density, the results depend on the discretization process and solver, and correct characterization of the materials used. Despite these challenges, FEM has become a reliable tool for analyzing soft and deformable robots.

The mechanical behavior of elastomers, mainly TPU and silicone, is highly nonlinear under load conditions, displaying effects such as hysteresis, relaxation, rate dependency and stress softening (both temporary and permanent) [5], [6]. To parametrize such behaviors, a variety of constitutive models have been proposed based on strain–energy density functions. For small to moderate strains, simple models such as linear elastic, Neo–Hookean, and Mooney-–Rivlin models offer reasonable accuracy. For materials undergoing large and complex strains, more sophisticated models such as the Ogden, Yeoh, and Arruda-–Boyce formulations are often employed. These models can then be used in simulation to compare stress–strain measurements with the experimental data [5], [7], [8]

Recent works have integrated FEM with optimization procedures to calibrate digital twins of soft robots in the open–source framework SOFA. In [9], researchers created an accurate inverse–kinematic control scheme for a self–healing, pneumatically actuated soft finger. By fitting several hyperelastic constitutive models to their experimental data, they found the Neo–Hookean and first–order Ogden laws to work the best due to the low strain deformations of the system. Using a high–density mesh of 64000 tetrahedrons and the Neo–Hookean material model in the FEM framework SOFA, they achieved a maximum position error below 1 mm when comparing nine marked points along the structure to those in the simulation. A similar approach has been used in [10] to model a pneumatically actuated soft continuum robotic arm made of silicone when external forces are applied. A less refined mesh of 3869 tetrahedra was used to achieve faster execution times, together with the default linear elastic model in SOFA. For a series of calibration tests (pressure actuation and disturbance estimation) the authors fixed the Poisson's ratio and optimized the Young's modulus to match the real results, finding discrepancies in the values, assumed to be caused by the fabrication process. For the validation tests they achieved satisfactory results for both the position and force estimations.

A more recent study [11] proposes a condensed FEM solution based on a learning approach of a neural network through simulation in SOFA as a framework for modeling, control and design soft manipulators. The condensed model

*denotes equal contribution

[1]Alberto Rodríguez–Sanz, Gerson Lipa, Jorge Muñoz and Concepción A. Monje are with RoboticsLab, Department of Systems Engineering and Automation, Universidad Carlos III de Madrid, Avda. Universidad 30, 28911, Leganés, Spain albertro@ing.uc3m.es

[2]Baptiste Rouquette is with the Department of Engineering, Sorbonne Université, 4 Pl. Jussieu, 75005, Paris, France baptiste.rouquette@etu.sorbonne-universite.fr

978-1-6654-5784-2/26/$31.00 ©2026 IEEE

is shown to find good values for either the Poisson's ratio or the Young's modulus in a soft pneumatic finger, depending on the desired actuation control. The researchers found the former parameter to be more critical in displacement control, as it is needed to accurately model the lateral deformations when longitudinal strains are applied on the finger. These studies collectively demonstrate that, in many soft robotic systems operating under small to moderate strains, simplified material models, such as the Neo–Hookean model, are sufficiently accurate for capturing the mechanical behavior.

The soft robotic neck considered in this study (Fig. 1) was previously analyzed in [12] and [13], where the influence of the mesh on the system's accuracy and performance, and the open–loop accuracy of FEM–based kinematic models compared to geometric approaches, were studied. In order to further match the behavior between the real platform and the digital twin, this work focuses on the characterization of the soft neck, which was manufactured from TPU filament with a Shore hardness of 82A (Recreus), with the goal of achieving accurate open–loop force control in a system which employs remarkably noisy DC motors.

The motivation for a more extensive system characterization stems from observed discrepancies between the manufacturer–provided mechanical values and those reported in prior experimental work [14], which highlighted the influence of printing parameters, infill patterns, and geometry on material behavior [15], [16], [17]. The soft robot under study in this paper was manufactured with a Prusa XL printer, using a 30% infill density with a gyroid pattern and 0º raster angle. Additionally, two vertical shells and four horizontal layers for both the top and bottom surfaces were used for printing the soft structure.

In this work, we present a FEM–based optimization framework for identifying the effective mechanical properties of a cable–driven soft robotic neck manufactured from TPU. The method combines force–displacement trajectories obtained from traction tests on a custom setup with simulations performed in the SOFA framework. A Sequential Model–Based Optimization (SMBO) strategy is used to estimate the Young's modulus and Poisson's ratio of a Neo–Hookean model by minimizing the discrepancy between real and simulated cable actuation. The resulting parameters enable a physically consistent digital twin of the neck, providing the foundation for improved control strategies.

II. METHODOLOGY

A. Experimental Setup

A uniaxial pulling test was performed using a universal testing machine (Instron 34SC–1) to characterize the mechanical response of the soft neck when actuated through its frontal cable. One end of the cable was attached to the upper grip of the UTM, while the opposite end remained fixed to the top mounting plate of the soft robot. Two steel ball–bearings (SKF 608ZZ), used as pulleys, were placed at equal height between both ends to guide the cable and produce an effective 180–degree redirection, as shown in Fig. 2.

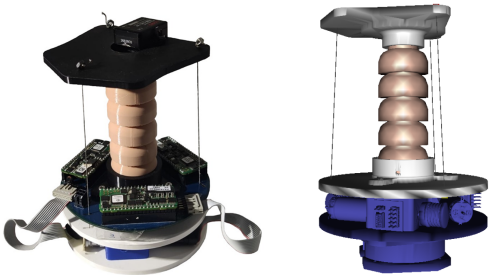

(a) Robotic platform (b) Digital twin in SOFA

Fig. 1: Overview of the soft neck platform studied in this work.

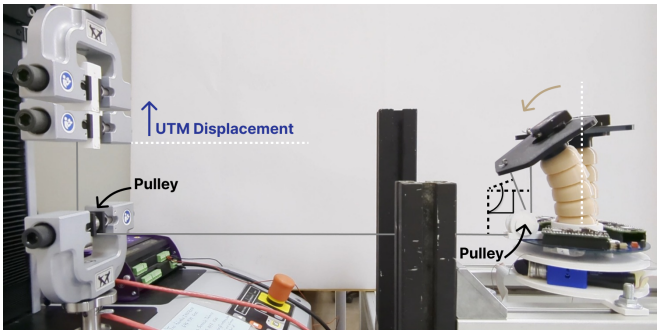

Fig. 2: Side view of the setup used in the uniaxial cable-pulling experiments.

Since the UTM measures the total pulling tension T_{UTM}, the effective force applied to the neck must be corrected to account for the dry friction in the two pulleys. Using the Euler–Eytelwein formulation, the tension transmitted to the neck is given by:

$$T_{neck} = T_{UTM}\, e^{-n\mu\theta}, \tag{1}$$

where n is the number of pulleys, μ is the friction coefficient between the UHMWPE cable and the ball–bearing surface, for which a value of 0.1 was considered [18], and $\theta = \pi$ is the wrap angle for each pulley. This correction is required to ensure consistency between the experimental measurements and the FEM–based simulations.

The soft neck was tested under two pulling speeds, 2 mm/s and 5 mm/s, and for two target cable displacements, 20 mm and 30 mm, which lie within the regular operating range of the neck. In terms of displacement, both trajectories remain within the robot's workspace, although the 30 mm case approaches its reachable limit. For each configuration, the UTM executed eight loading–unloading cycles, reaching the lower force limit of 0.1 N, while recording force and displacement at 0.01 s intervals. In parallel, an IMU mounted on the back of the top plate measured roll and pitch angles at the same sampling rate.

Only one printed specimen was used throughout all tests. Prior to data collection, the neck was subjected to a short preconditioning routine to mitigate Mullins–type stress softening [5]. The resulting force–displacement curves (Fig. 3) exhibit the characteristic hysteresis loops of TPU elastomers.

Furthermore, a pronounced softening is observed between the first and second loading curves, caused by viscoplastic relaxation, and followed by a more stable response over subsequent cycles. Despite these viscoelastic and viscoplastic effects, the loading branch remains approximately linear across cycles, which supports the use of a Neo–Hookean hyperelastic model to represent the material behavior during force–controlled cable actuation.

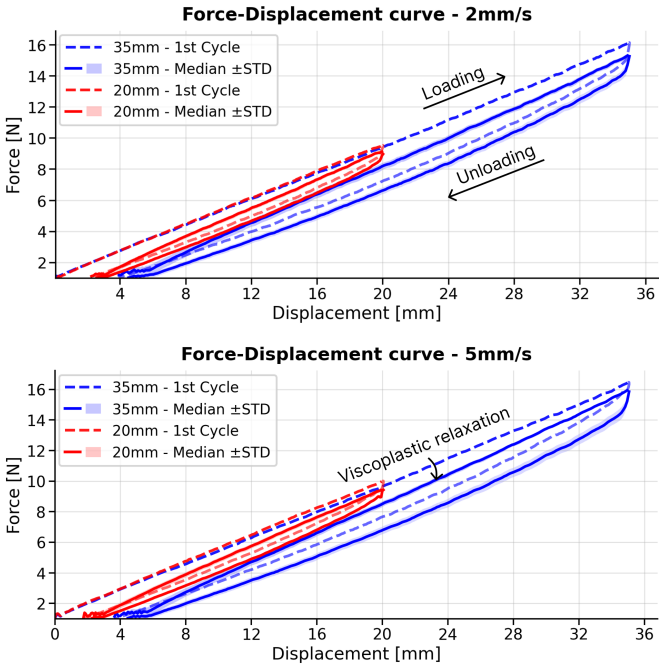

Fig. 3: Force–displacement results from the cyclic traction tests at different target displacements and pulling speeds.

B. Scene Description

The SOFA scene consists of a digital twin of the soft–neck platform composed of two main components: a volumetric FEM model of the neck and a rigid body representing the top mounting plate. The bottom of the neck is fixed to the global reference frame, corresponding to the real platform's rigid electronics base, while the top plate is modeled as a *Rigid3D* object. This rigid body is attached to the deformable neck through a *MechanicalMapping*, ensuring that its motion is fully determined by the deformation of the soft structure.

The neck geometry is discretized into approximately 4000 tetrahedral elements generated using a Delaunay–based meshing strategy via the Gmsh library. This resolution was selected as a compromise between accuracy and computational cost, following the mesh refinement criteria evaluated in [12]. The simulation uses an implicit Euler scheme for time integration, with Rayleigh damping coefficients of 0.2 for stiffness and 0.1 for mass to stabilize the system by modeling energy dissipation.

The resulting linear system at each step is solved using the *SparseLDL* solver, which is well suited for the sparse matrices arising from FEM formulations. Cable actuation is implemented through the *CableConstraint* component, which

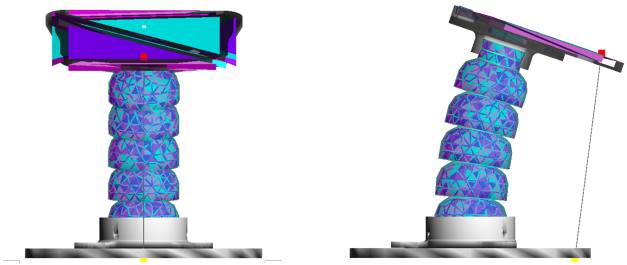

(a) Front view (b) Side view

Fig. 4: FEM model of the soft neck actuated through a cable constraint for a pitch inclination of 0.32 rad.

computes the cable tension and resulting displacements. The constraint is resolved using a Projected Gauss–Seidel (PGS) method with a maximum of 500 iterations and a convergence tolerance of 1×10^{-9}. Only the frontal cable is modeled, mirroring the configuration used during the UTM traction experiments.

Material behavior is implemented through the *TetrahedronHyperelasticityFEMForceField* component, which applies the Neo–Hookean constitutive law. The optimized material parameters obtained in this study are directly incorporated into this force field to replicate the real mechanical response under force–controlled cable actuation. However, it is important to note that the Neo–Hookean model only provides an approximation of the behavior of the real structure. To achieve a more accurate simulation of the soft robot, it is necessary to fine–tune both the mesh density and the solver settings. [1]

C. Hyperelastic Constitutive Model

The soft neck is modeled using a Neo–Hookean hyperelastic formulation, which offers a good balance between accuracy and computational efficiency for the small to moderate strains observed during cable actuation. Although more complex models (e.g., Ogden, Yeoh, or Arruda–Boyce) can capture large–strain or rate–dependent behavior, previous studies on similar soft robotic structures have shown that the Neo–Hookean law provides sufficiently accurate results under comparable deformation ranges [9], [10].

The formulation is expressed in terms of the Lamé parameters, λ and μ, which are related to the conventional Young's modulus E and Poisson's ratio ν by:

$$\mu = \frac{E}{2(1+\nu)}, \tag{2}$$

$$\lambda = \frac{E\nu}{(1+\nu)(1-2\nu)}. \tag{3}$$

As ν approaches 0.5, the material becomes nearly incompressible and the parameter λ increases sharply, which is known to induce numerical instabilities in FEM simulations. For this reason, values exactly equal to 0.5 are avoided in practice.

[1]The simulation code developed for this work is available at this repository.

D. Material Optimization

To determine the effective Young's modulus and Poisson's ratio, we adopted an optimization approach aimed at minimizing the error between the cable displacements recorded on the test bench and those obtained from the simulated model under force control. For this task, we employed a Sequential Model–Based Optimization (SMBO) method using the Optuna framework. This choice is justified by the low dimensionality of the problem: only two material parameters are estimated, and the associated response surface is sufficiently smooth that more elaborate optimization strategies or extensive hyperparameter tuning are unnecessary. The optimization was run using Optuna's default SMBO settings for 1000 trials; in this setting, repeated runs did not show evidence of multiple local minima, consistently converging to similar parameter values.

The optimization was carried out using the following cost function:

$$f_c = \alpha \cdot error_{force} + \beta \cdot error_{\theta}, \tag{4}$$

where α and β are the weights assigned to the cable–force error and pitch–angle error, respectively. Pitch was weighted more strongly ($\alpha = 0.3$, $\beta = 1$) because angular measurements are less affected by cable friction and boundary effects than force readings, and therefore provide a more reliable indication of the global mechanical response.

The search space for the material parameters was defined to cover the typical ranges reported for printed TPU structures and to ensure numerical stability in the FEM solver. Young's modulus was restricted to $E \in [0.1, 40]$ MPa, spanning values from soft printed geometries to stiffer effective responses, while Poisson's ratio was limited to $\nu \in [0.4, 0.4999]$ to avoid instabilities near the incompressible limit.

III. Optimization Results

The optimization process was applied to four different experimental configurations. In all cases, the algorithm successfully converged to a pair of mechanical parameters, Young's modulus (E) and Poisson's ratio (ν), that minimized the cost function.

The four experiments exhibited consistent trends in the identification of the material parameters, as summarized in Table I. Young's modulus showed a clear dominance in the optimization process, with importance values between 0.926 and 0.972. In contrast, Poisson's ratio had a much smaller influence across all tests, remaining below 0.08. Figure 5 shows the optimization results for the four experiments.

Experiment 1 (20 mm – 2 mm/s) produced the softest response, with $E = 1.2$ MPa and a nearly incompressible Poisson's ratio of $\nu = 0.497$. Increasing the loading rate in Experiment 2 (20 mm – 5 mm/s) resulted in a higher modulus ($E = 1.9$ MPa) and a slightly lower ν. Experiment 3 (35 mm – 2 mm/s) yielded the highest modulus ($E = 2.3$ MPa), while Experiment 4 (35 mm - 5 mm/s) produced a value similar to that of Experiment 2. These results reinforce the consistent predominance of Young's modulus in the cost function.

TABLE I: Summary of optimized parameters and variable importance for the four experiments.

Experiment	E (MPa)	ν	Imp. E	Imp. ν
1	1.2	0.497	0.972	0.028
2	1.9	0.446	0.926	0.074
3	2.3	0.431	0.9994	0.0006
4	1.7	0.488	0.972	0.028

To validate the obtained parameters, each configuration was simulated and compared against the experimental force and pitch measurements for the full trajectory. Figure 6 shows the evolution of these signals, and Table II summarizes the RMS detrended errors. Among all cases, Experiment 3 provided the closest match to the reference force curve, with an RMS error of 0.1404. This value aligns with the observations reported in [19], where the transverse mechanical response of printed TPU converged toward a Poisson's ratio close to 0.48 after cyclic loading. Differences between the remaining configurations were more noticeable in force, but all experiments produced similarly low pitch–angle errors.

Experiment	Force RMSE (detr.)	Pitch RMSE (detr.)
1	0.1588	0.0135
2	0.2814	0.0136
3	0.1404	0.0136
4	0.1425	0.0136

TABLE II: RMS detrended errors for different configurations of E and ν.

The optimized Young's modulus values (1.2–2.3 MPa) are lower than those typically reported for bulk TPU 82A, whose tensile modulus commonly lies in the 8–12 MPa range for solid specimens. This difference is expected because the neck is not manufactured as a solid body: its stiffness is strongly influenced by the printing parameters, including the 30% gyroid infill, the shell configuration, and the thickness of the top and bottom layers. These factors reduce the effective stiffness of the printed part relative to the bulk material.

Equation (5) describes the reduction of stiffness by expressing the effective modulus as a function of the material modulus and the relative density of the printed structure.

$$E_{\text{eff}} = E_{\text{bulk}}\, \phi^{\gamma} \tag{5}$$

where ϕ is the infill fraction and γ is an empirical exponent that depends on the overall stiffness reduction associated with the printing strategy. For typical FDM geometries, values of γ between 1.2 and 1.6 have been reported, which places the expected range of E_{eff} between 1.5 and 4 MPa for a 30% infill. The optimized values obtained in this work are therefore consistent with these estimates and with previously reported measurements for printed TPU.

Regarding Poisson's ratio, the identified values (0.43–0.49) closely match the values obtained in studies analyzing the nonlinear and rate–dependent transverse behavior of TPU under cyclic loading [20], [21], [22]. The upper limit was constrained to 0.499 to avoid numerical instabilities typically encountered when approaching the nearly incompressible regime in hyperelastic simulations.

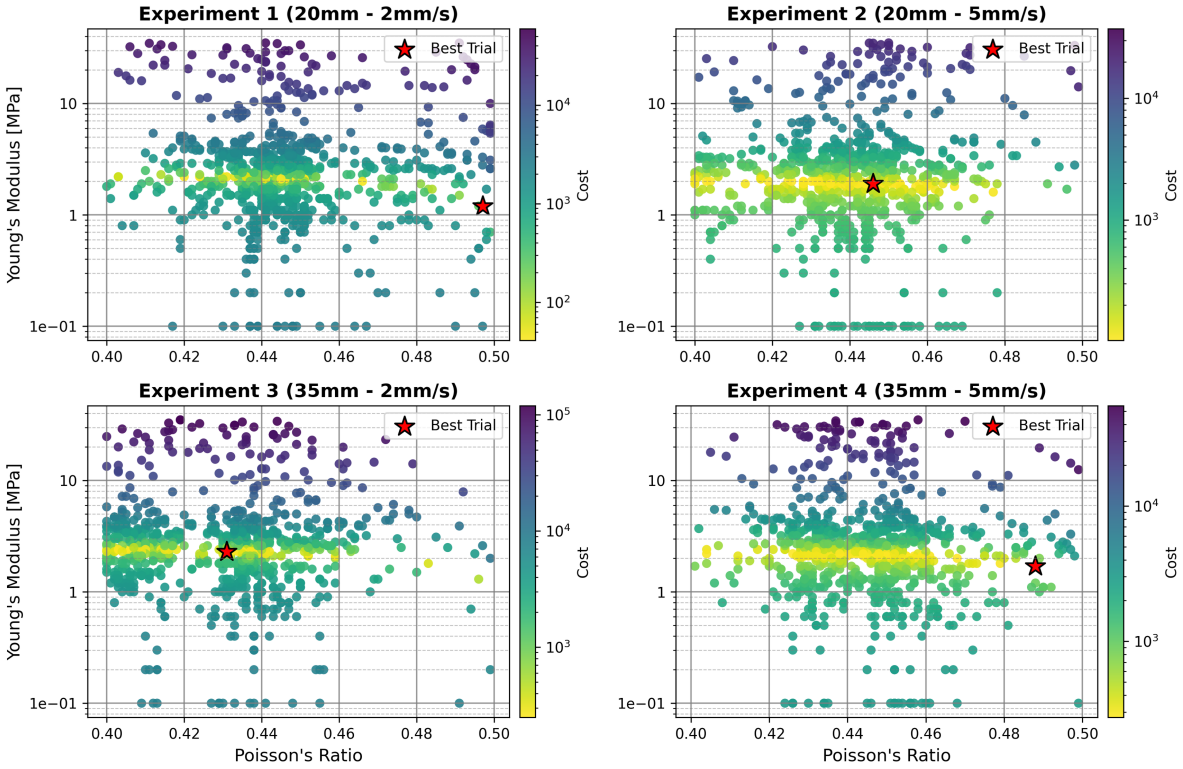

Fig. 5: Optimization results for all four experiments.

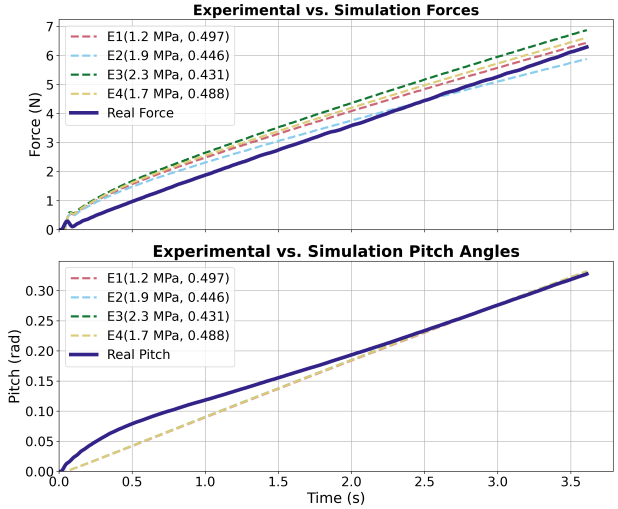

Fig. 6: Simulated and experimental force and pitch trajectories using the optimized parameters.

Overall, the optimized parameters are physically reasonable for a printed TPU structure and reflect both the geometric characteristics of the specimen and the approximations inherent to the FEM model.

IV. CONCLUSIONS

This work presented a simulation–based framework for identifying the effective mechanical properties of a cable–driven soft robotic neck. Using a Neo–Hookean formulation within the SOFA framework and focusing on the loading phase of the experimental traction cycles, it was possible to extract the dominant elastic response of the printed TPU structure. The optimization procedure, implemented through Optuna, consistently converged to Young's modulus and Poisson's ratio values that reproduced the experimental force and pitch measurements with satisfactory accuracy. Among these configurations, the one obtained in Experiment 3 provided the closest match to the recorded trajectories.

Overall, the results demonstrate that the proposed workflow offers a practical and reliable approach for calibrating soft robotic structures when direct material characterization is limited or impractical. The framework provides a consistent method to determine effective mechanical parameters for use in simulation-based analysis, prototyping, and design refinement.

Looking ahead, several extensions of this work are planned. A more detailed experimental characterization including additional loading speeds, multi–cable actuation, external load conditions, and long–term cyclic tests would help capture the rate–dependent and viscoplastic behavior reported for TPU in previous studies. Incorporating these effects into the model, together with refined mesh strategies or alternative constitutive laws, may further improve the accuracy of the simulation. Once fully calibrated, the digital twin developed here will offer a solid foundation for exploring advanced control strategies, including real–time, model–based, or adaptive force–position control of the soft neck.

ACKNOWLEDGMENT

The research leading to these results has been partially funded by the project ADAPTA, reference PLEC2023–010218, funded by MICIU /AEI /10.13039/501100011033; SIROCO, reference PID2023–147343OB–I00, funded by MICIU /AEI /10.13039/501100011033 and by FEDER, EU; and the R&D activity program with reference TEC–2024/TEC–62 and acronym iRoboCity2030–CM, granted by the Community of Madrid through the Directorate General for Research and Technological Innovation, under Order 5696/2024.

REFERENCES

[1] R. J. WebsterIII and B. A. Jones, "Design and kinematic modeling of constant curvature continuum robots: A review," *The International Journal of Robotics Research*, vol. 29, no. 13, pp. 1661–1683, 2010.

[2] D. Trivedi, C. D. Rahn, W. M. Kier, and I. D. Walker, "Soft robotics: Biological inspiration, state of the art, and future research," *Applied Bionics and Biomechanics*, vol. 5, no. 3, p. 520417, 2008.

[3] X. Wang, J. J. Dabrowski, J. Pinskier, L. Liow, V. Viswanathan, R. Scalzo, and D. Howard, "Pinn-ray: A physics-informed neural network to model soft robotic fin ray fingers," in *2024 IEEE/RSJ International Conference on Intelligent Robots and Systems (IROS)*, pp. 247–254, 2024.

[4] M. Dubied, M. Y. Michelis, A. Spielberg, and R. K. Katzschmann, "Sim-to-real for soft robots using differentiable FEM: Recipes for meshing, damping, and actuation," *IEEE Robotics and Automation Letters*, vol. 7, no. 2, pp. 5015–5022, 2022.

[5] S. I. Reyes, M. F. Vassiliou, and D. Konstantinidis, "Experimental characterization and constitutive modeling of thermoplastic polyurethane under complex uniaxial loading," *Journal of the Mechanics and Physics of Solids*, vol. 186, p. 105582, 2024.

[6] C. Yuan, M. Z. Rong, and M. Q. Zhang, "Self-healing polyurethane elastomer with thermally reversible alkoxyamines as crosslinkages," *Polymer*, vol. 55, no. 7, pp. 1782–1791, 2014.

[7] L. Lang, R. Antunes, T. A. Dutra, M. L. d. Aguiar, N. Pereira, and P. D. Gaspar, "Mechanical characterization and computational analysis of TPU 60A: Integrating experimental testing and simulation for performance optimization," *Materials*, vol. 18, no. 2, 2025.

[8] C. Schumacher, E. Knoop, and M. Bächer, "Simulation-ready characterization of soft robotic materials," *IEEE Robotics and Automation Letters*, vol. 5, no. 3, pp. 3775–3782, 2020.

[9] P. Ferrentino, S. K. Tabrizian, J. Brancart, G. V. Assche, B. Vanderborght, and S. Terryn, "FEA-based inverse kinematic control: Hyperelastic material characterization of self-healing soft robots," *IEEE Robotics & Automation Magazine*, vol. 29, no. 3, pp. 78–88, 2022.

[10] B. G. Cangan, S. E. Navarro, B. Yang, Y. Zhang, C. Duriez, and R. K. Katzschmann, "Model-based disturbance estimation for a fiber-reinforced soft manipulator using orientation sensing," in *2022 IEEE/RSJ International Conference on Intelligent Robots and Systems (IROS)*, pp. 9424–9430, 2022.

[11] T. Navez, E. Ménager, P. Chaillou, O. Goury, A. Kruszewski, and C. Duriez, "Modeling, embedded control, and design of soft robots using a learned condensed FEM model," *IEEE Transactions on Robotics*, vol. 41, pp. 2441–2459, 2025.

[12] G. M. Lipa, A. Rodríguez-Sanz, C. A. Monje, J. Muñoz, and S. Martínez, "Refinamiento de mallas para simulaciones en SOFA framework: Equilibrio entre comportamiento dinámico y eficiencia computacional," *Simposio CEA de Robótica, Bioingeniería, Visión por Computador y Automática Marina*, vol. 1, no. 1, 2025.

[13] G. M. Lipa Noriega, A. Rodríguez-Sanz, J. Muñoz Yáñez-Barneuvo, S. Martínez de la Casa Díaz, and C. A. Monje Micharet, "Inverse kinematics modeling of a cable-actuated soft robotic neck in SOFA," *Jornadas de Automática*, vol. 46, 2025.

[14] A. Rodríguez-Sanz, C. Sánchez Hernández, S. Martínez, and C. A. Monje, "Influencia de la orientación del patrón de relleno en las propiedades mecánicas del TPU de dureza 82A," *Simposio CEA de Robótica, Bioingeniería, Visión Artificial y Automática Marina*, vol. 1, no. 1, 2025.

[15] S. Nace, J. Tiernan, D. Holland, and A. Ní Annaidh, "A comparative analysis of the compression characteristics of a thermoplastic polyurethane 3D printed in four infill patterns for comfort applications," *Rapid Prototyping Journal*, vol. 27, pp. 24–36, 12 2021.

[16] H. Sadaghian, B. Dadmand, M. Pourbaba, S. Jabbari, and J. H. Yeon, "The effect of size on the mechanical properties of 3D-printed polymers," *Sustainability*, vol. 16, no. 1, 2024.

[17] V. M. Bruère, A. Lion, J. Holtmannspötter, *et al.*, "The influence of printing parameters on the mechanical properties of 3D printed tpu-based elastomers," *Progress in Additive Manufacturing*, vol. 8, pp. 693–701, 2023.

[18] R. Marissen, "Design with ultra strong polyethylene fibers," *Materials Sciences and Applications*, vol. 2, pp. 319–330, 2011.

[19] Y. Xu and J.-Y. Juang, "Measurement of nonlinear poisson's ratio of thermoplastic polyurethanes under cyclic softening using 2D digital image correlation," *Polymers*, vol. 13, no. 9, p. 1498, 2021.

[20] D. M. Haid, O. Duncan, J. Hart, and L. Foster, "Characterisation of thermoplastic polyurethane (tpu) for additive manufacturing," in *spinfortec2022: Tagungsband zum 14. Symposium der Sektion Sportinformatik und Sporttechnologie der Deutschen Vereinigung für Sportwissenschaft (dvs), Chemnitz, 29.–30. September 2022*, 2022. [Online]. Available: urn:nbn:de:bsz:ch1-qucosa2-807862.

[21] H. Lee, R.-i. Eom, and Y. Lee, "Evaluation of the mechanical properties of porous thermoplastic polyurethane obtained by 3d printing for protective gear," *Advances in Materials Science and Engineering*, vol. 2019, no. 1, p. 5838361, 2019.

[22] H. Qi and M. Boyce, "Stress–strain behavior of thermoplastic polyurethanes," *Mechanics of Materials*, vol. 37, no. 8, pp. 817–839, 2005.